SSRG International Journal of Mechanical Engineering
ISSN: 2348-8360/ https://doi.org/10.14445/23488360/IJME-V12I3P102

Volume 12 Issue 3, 28-35, March 2025

Original Article

Effect of Boundary Layer Trips on Low-Velocity Wind Turbine Blade: A Computational Study

Suhas B.G[1*], Anil Chandra A.R[2], Prema V.[3], Sreejith B.K.[4] , Abdulrajak Buradi[5], Kiran Kumar K.U.[6]

[1,2,6]*Department of Mechanical Engineering, B.M.S. College of Engineering, Bull Temple Road, Bengaluru, Karnataka, India.*
[3]*Department of Electrical and Electronics Engineering, B.M.S. College of Engineering, Bull Temple Road, Bengaluru, Karnataka, India.*
[4]*Department of Mechanical Engineering, A.J Institute of Engineering and Technology, Mangaluru, Dakshina Kannada, Karnataka, India.*
[5]*Department of Mechanical Engineering, Nitte Meenakshi Institute of Technology, BSF Campus, Yelahanka, Bengaluru, Govindapura, Karnataka, India.*

[*]*Corresponding Author : suhas_bg@yahoo.co.in*

Received: 04 January 2025 Revised: 03 February 2025 Accepted: 02 March 2025 Published: 29 March 2025

Abstract - *This study focuses on designing wind turbines that can efficiently generate energy from low wind velocities. It investigates airfoils operating at low Reynolds Numbers (Re <500,000), where their performance often suffers due to Laminar Separation Bubbles (LSBs). The research applies passive methods to mitigate this effect and enhance blade efficiency. A site-specific analysis identified the design wind speed as 7.25 m/s at a hub height of 10 meters, adhering to IEC standards. The passive flow control method was employed to reduce LSBs and drag, thereby boosting the aerodynamic performance of the FX 63-137 airfoil. A 2D computational study evaluated the influence of rectangular-shaped BLTs on airfoil performance. The analysis considered various angles of attack and wind speeds (5.15, 7.25, and 10 m/s). The introduction of BLTs reduced total drag by approximately 14%. The lift-to-drag ratio (Cl/Cd) increased by roughly 12.3% at the design wind speed. The numerical analysis showed strong agreement with experimental data available in the literature, demonstrating the validity of the approach. This research confirms the effectiveness of boundary layer trips in improving aerodynamic performance under low wind speed conditions. The findings support the potential of this method to enhance the efficiency of small-scale wind turbines in regions with moderate wind resources.*

Keywords - *Boundary Layer Trips, Laminar Separation Bubble, Passive techniques, Power generation, Small speed wind turbine.*

1. Introduction

The global energy demand is steadily increasing due to rapid population growth and industrial development. Conventional energy sources, however, have significant adverse effects on the climate. Projections estimate that the total installed capacity of renewable energy production will rise by 218 GW in 2023. Between 2020 and 2025, the expected growth in global electricity demand is anticipated to be met primarily by renewable sources (Dias et al., 2022; IEA Publications, 2020). Among renewable energy sources, wind energy stands out as one of the fastest-growing resources. Wind turbines are categorized into two types: Large-Scale Wind Turbines (LSWT) and Small-Scale Wind Turbines (SSWT). Several distinctions exist between them, most notable being their operational wind speed range and Reynolds number. For instance, electrifying remote regions often involves areas with low wind speeds, which fall below the operating range of large wind turbines (Jeff et al., 2022). According to IEC 61400-2, the safety standard for small wind turbines, turbines with a swept area of less than 200 m² are classified as SSWTs (IEC, 2013). The key difference is that small turbine blades operate at low Reynolds numbers ($Re <$ 500,000) across their entire span. The power output of a wind turbine depends on factors including the cube of the wind speed (U_α), the square of the rotor radius (r) and the aerodynamic performance of the airfoil, such as the lift-to-drag ratio (C_l/C_d) of the blades. For SSWTs, both rotor radius and wind velocity are limited due to design constraints. Therefore, enhancing blade performance by optimizing the (highest C_l/C_d ratio) ratio is crucial for improving power production. This can be achieved either by increasing lift C_l or decreasing drag C_d. While an increased Angle of Attack (AOA) can improve lift, providing a higher AOA at design conditions is challenging because most SSWTs are either constant-pitch or stall-regulated. Moreover, at higher AOAs, drag increases significantly, which reduces the C_l/C_d ratio.

Another effective approach involves minimizing drag. Airfoil drag mainly arises from viscous drag and pressure drag. While thin airfoils can lower pressure drag, structural limitations restrict the extent to which thickness can be reduced. At low Reynolds numbers, the formation of Laminar Separation Bubbles (LSBs) due to Adverse Pressure Gradients (APG) further increases total drag significantly, along with viscous drag, as depicted in Figure 1.

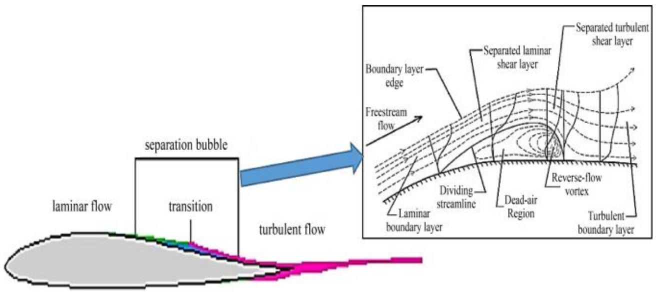

Fig. 1 Laminar separation bubble - Zoomed view (Jahanmiri et al. 2011)

The constant pressure line depicts laminar separation, while a sudden pressure rise signifies the re-energization of the boundary layer, often referred to as the transition region, before it attaches to the airfoil surface. The length of the separation bubble is highly dependent on the Reynolds number (Re). An increase in the Angle of Attack (AOA) intensifies the Adverse Pressure Gradient (APG), causing the separation bubble to move upstream. Beyond the critical angle of attack, the flow fully separates. Reducing the size of the separation bubble is essential for controlling boundary layer flow and improving the aerodynamic performance of low-Re airfoils (Musial et al., 1988; Rodriguez et al., 2022). The Laminar Separation Bubble (LSB) on the airfoil can be identified and located through the surface pressure coefficient (Cp) distribution. Effective flow separation control strategies can minimize the drag associated with LSB. These controls can be active, relying on energy-driven methods like electrically operated actuators, unsuitable for Small-Scale Wind Tunnels (SSWT), or passive, which do not require external energy. Among passive methods, Boundary Layer Trips (BLTs) have gained prominence in enhancing airfoil performance. Researchers have extensively studied BLTs as a passive control technique for reducing LSB formation (Sreejith et al., 2018; Dong et al., 2018; Kamada et al., 2016; Mitra et al., 2015; Khan et al., 2020). Currently, one of the most effective methods for eliminating LSB involves mechanical BLTs such as trip cables, zigzag tape, and simple trips. Sreejith and Sathyabhama (2018) conducted numerical simulations on the E216 airfoil, demonstrating that BLTs induced turbulence, eliminated LSB, and enhanced aerodynamic performance.

The characteristics of LSB formation vary depending on the airfoil-Reynolds number combination. Limited studies have focused on LSB formation within the Reynolds number range of 50,000 to 100,000. Notable differences exist between LSB behavior at low Re (30,000–100,000) and higher Re (100,000–300,000). Similarly, the FX 63-137 airfoil performance with and without BLTs exhibits distinct behavior in these Reynolds number ranges (Mitra et al., 2015). The present study offers a novel perspective that explores the influence of rectangular-shaped BLTs on the LSB of airfoils within the Reynolds number range of 50,000 to 100,000. Recognized for their ease of fabrication, rectangular BLTs are the centrepiece of the research. The study examines their impact on LSB characteristics through numerical simulations, targeting a reduction in bubble length to improve airfoil performance.

2. Methodology

2.1. Aerofoil Selection

The annual average wind speed at the proposed installation site was estimated using the Global Wind Atlas and WAsP® software. This data was then used to determine the necessary size of the wind turbine blade to achieve the desired power output. A preliminary airfoil analysis conducted with QBlade® software led to the selecting of an appropriate airfoil for the blade profile. Further computational work was carried out using commercial software. The proposed wind turbine will be located near Manchenahalli Lake in Chikballapura District, Karnataka (13.50°N, 77.611°E). Figure 2 depicts the Weibull probability distribution of wind speed at the site, generated by WAsP® software. The average wind speed (V_{avg}) at the location was measured to be 5.15 m/s, with the maximum probable wind speed recorded at 3.57 m/s, as shown in Figure 2. Applying the maximum probability of occurrence, the design wind speed was determined to be 7.25 m/s at a hub height of 10 m, following IEC standards (IEC, 2013).

$$V_{design} = 1.4 \times V_{avg} \tag{1}$$

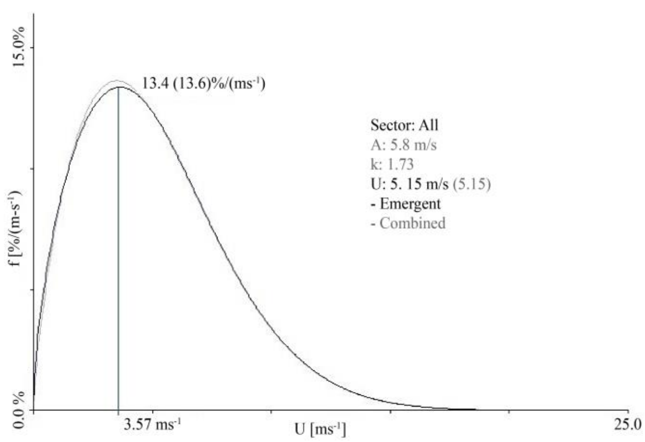

Fig. 2 Weibull probability distribution of wind speed

The performance of small wind turbines at low wind speeds is strongly influenced by the choice of airfoil for the blade cross-section. Concluding from existing literature (Miley S. et al., 1982; Ronit et al., 2012), seven airfoils suitable for low-Reynolds-number applications were shortlisted. These airfoils were evaluated using QBlade® at an operational Reynolds number (Re) of 164,000, corresponding to a wind velocity of 7.5 m/s and an angle of attack (α) ranging from -6° to 20° (Suhas et al., 2023). This Re value reflects the running torque at 30% of the distance from the blade tip (Kelele et al., 2022). Notably, the FX63-137 airfoil achieved the highest C_l/C_d ratio and had the greatest maximum thickness among the seven, at 13.7% of the chord length. Wind tunnel tests by Selig and McGranahan (2004) on six airfoils, including FX63-137, revealed that while bubble drag adversely affected performance at very low Re (100,000), drag on the FX63-137 decreased significantly at 150,000 Re and improved further at 500,000 Re. Considering these parameters, the FX63-137 airfoil was selected as the optimal choice for the blade.

2.2. Geometric Modeling

The effect of the BLT on the performance of the FX63-137 airfoil was analyzed using a 2D geometry. Figure 3 illustrates the computational fluid domain along with the dimensions and boundary conditions employed in the study. According to blade element calculations by Manwell et al. (2010), the majority of the starting torque is generated near the hub. Consequently, the root section of the blade, with a chord length of 129.15 mm, was selected for simulation. A rectangular boundary layer trip with dimensions of 2 mm width and 0.3 mm height was applied, as depicted in Figure 3.

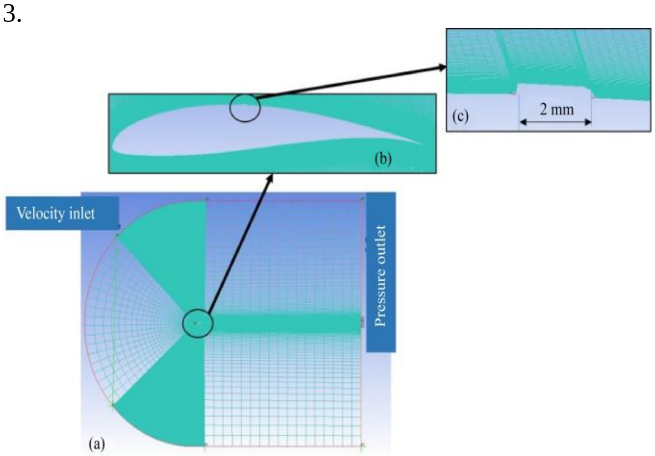

Fig. 3 Computational domain with, (a) structured grid and boundary conditions, (b) highlighting 2D blade profile with, and (c) rectangular shape BLT, used in the study.

Further details are discussed in Section 3.3. To ensure a fully developed flow, the computational domain should extend 9 times the chord length (9c) upstream of the airfoil and 15 times the chord length (15c) downstream (Sreejith et al., 2020). Adequate space must also be allocated around the airfoil to prevent interactions between the flow disturbances generated by the airfoil and the domain boundaries.

2.3. Meshing the Computational Fluid Domain, Boundary Conditions and Turbulence Model

A structured grid with a C-type mesh was created for the simulation, as depicted in Figure 3. The computational domain consists of 284,272 grid cells, determined through a grid independence study. The mesh for both the baseline airfoil and the airfoil with a BLT is nearly identical, except for a small shape modification due to the trip. A finer mesh resolution is employed in the vicinity of the airfoil to ensure higher computational accuracy in this critical region. The airfoil is subjected to a no-slip boundary condition, with a velocity inlet boundary condition specified at the domain's entrance. Symmetry is applied to the walls, and a pressure outlet boundary condition is used at the exit. The free stream temperature for calculating fluid characteristics is set to 300 K, equivalent to the ambient temperature. Air is chosen as the fluid material with a 1.225 (kg m-3) density and a dynamic viscosity of 1.7894×10^{-5} (kg s^{-1} m^{-1}). The flow is treated as incompressible with a turbulence intensity level of 5%. The coupled solution method, known for its robustness and efficiency in steady-state single-phase flows, is adopted (Matsson et al., 2022; Lili et al., 2020). Spatial discretization is performed using the second-order upwind method. This technique converts continuous functions (representing the true response to a system of differential equations in CFD) into discrete functions with defined solution values in space and time. The momentum and energy equations are spatially discretized during the simulations using this second-order upwind approach, ensuring accuracy and stability (Matsson et al., 2022; Lili et al., 2020).

To meet the requirements of the turbulence models used, the height of the first grid cell nearest to the airfoil surface is designed to achieve a y+ value of less than 1. The spatial gradient is calculated using the least square cell-based method, ensuring precision. The convergence criteria are set with a residual target of 10^{-5}. Turbulent models are employed in CFD simulations to accurately predict and simulate the development of turbulence in most real-world flow scenarios. These turbulence models predict the statistical growth of turbulent flows. In the present work, the Langtry-Menter 4-equation Transitional SST Model or γ - Re_θ - SST model [Dong et al. 2019] is used as the turbulence model. Its foundation is the two-equation k - ω SST model. It is supplemented by two further equations that characterize the laminar-turbulent transition process: one for intermittency (γ) and one for transitional Reynolds number ($Re_{\theta t}$). More information regarding the Langtry-Menter 4-Equation Transitional SST Model or γ - Re_θ - SST model is present in the literature (Menter et al. 2006). The simulation is carried out for Re 164,000 at 7.25 m s^{-1}.

2.4. Grid Independence Study

Four sets of meshes with 60,000 to 549,000 elements each are used for the grid independence test. Grid independence tests were carried out for both baseline airfoil and airfoil with BLT. For grid consistency, the parameters C_l and C_d are examined. Figure 4 shows the results of a grid independence study done for a baseline airfoil with a 5.5° angle of attack at 5.15 m/s wind speed. After approximately 284,272 grid cells, the C_l and C_d values showed no significant variation, making this mesh size the optimal choice for further analysis.

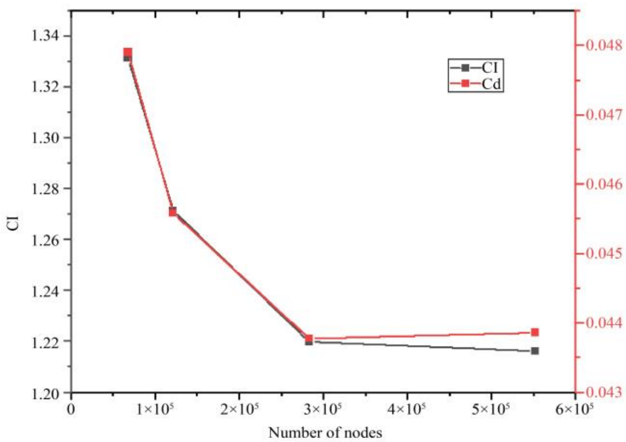

Fig. 4 Effect of the grid cell count on the lift and drag coefficient of the base airfoil at 5.5° AOA at a wind speed of 5.15 m s^{-1}

2.5. Validation of Numerical Simulation

The steady-state CFD simulation methodology for determining the position of LSB formation and reattachment on the FX63-137 airfoil is validated using the experimental results of Dong et al.. The variation of coefficient of pressure (C_p) on the airfoil at Re 200,000 at AOA 4° obtained from the numerical analysis is superimposed with available results in the literature and is shown in Figure 4.

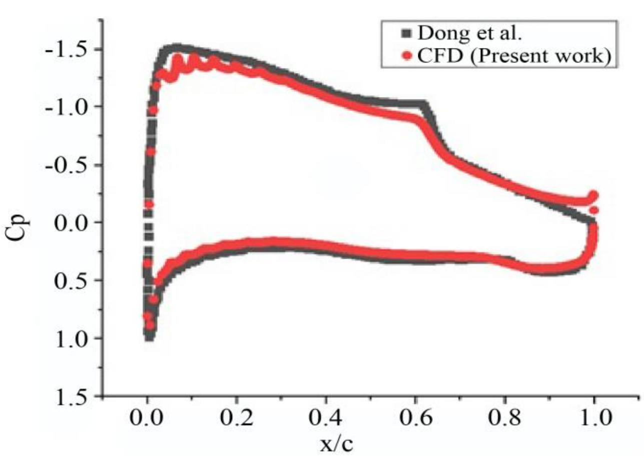

Fig. 5 Comparison of variation of C_p on the airfoil for *Re* 2 x 10^5 at AOA 4° obtained from present work and Dong et al. (2019)

In the present result and the literature, the flow separation happens at 0.42*c* from the leading edge and reattaches at 0.65*c*, as shown in Figure 5. The figure shows that the present result is in good agreement with the experimental results of Dong et al.

3. Results and Discussion

3.1. Surface Pressure Distribution

The distribution of C_p over the airfoil at different wind speeds is shown in Figure 6. A pressure plateau is seen on the suction side of the airfoil for all three wind speeds (5, 7.25, and 10 m s^{-1}), which shows that LSB is present in all three wind conditions and is detrimental to power production. An abrupt change in C_p is followed by a constant pressure regime, which makes up the hump. “S” represents the beginning of flow separation from the airfoil followed by a constant pressure until the transition happens at “T”. Mixing the fluid and the separated laminar boundary layers takes place after the constant pressure regime (point T); the shear layer is re-energized from this fluid and quickly raises the pressure, causing an abrupt change in C_p (Genc et al. 2019).

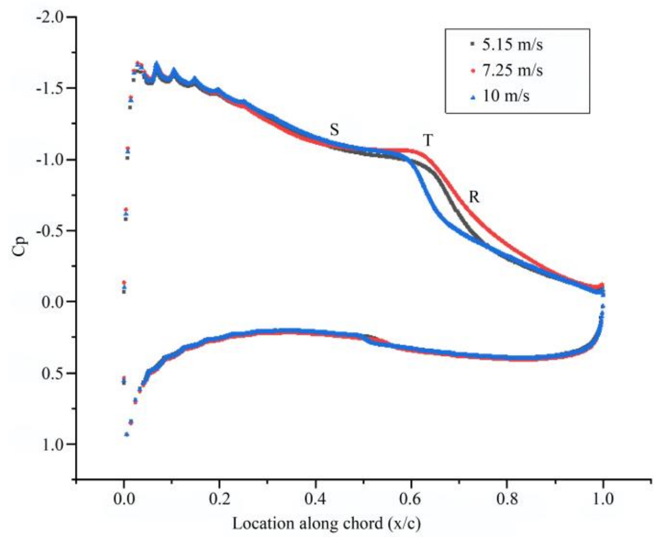

Fig. 6 The distribution of C_p over the airfoil at various wind speeds without BLT

This area is regarded as a transitional area (T-R). As an attached flow, the energetic shear layer reattaches to the airfoil surface. The point of reattachment is defined as the location where the actual pressure distributes and an inviscid flow coincides (point R). The term “LSB” refers to this flow separation and reattachment event, which starts at 0.46*c* (*S*) and finishes at 0.73*c (R)* from the leading edge depicts the LSB region. Figure 7 (a), (b), and (c) illustrates the pressure distribution across the airfoil surface, with and without a boundary layer trip (BLT), at an Angle of Attack (AOA) of 5.5° and varying wind speeds. The figures reveal a smooth pressure gradient on the upper surface of the airfoil when the BLT is applied, indicating the elimination of the Laminar Separation Bubble (LSB). The BLT induces a localized flow restriction in the suction region, causing a sharp rise in C_p. Apart from this localized effect, the C_p distribution remains smooth, demonstrating that the BLT effectively transitions the flow from laminar to turbulent. For the base airfoil at an AOA of 5.5°, a numerical analysis (Figure 8) identifies the LSB location at 0.46c from the leading edge, consistent across all velocities. The placement of the BLT ahead of this point, at 0.41c from the leading edge, successfully prevents LSB formation, confirming its effectiveness in improving the airfoil's aerodynamic performance.

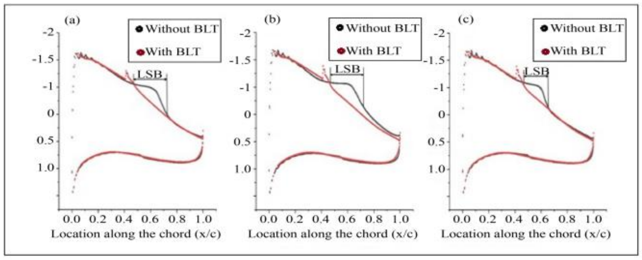

Fig. 7 Comparison of C_p for AOA 5.5º at (a) 5.15, (b) 7.25, and (c) 10 m s^{-1} with and without BLT and without BLT.

3.2. Surface Velocity Distribution

The flow pattern around the laminar separation bubble at different wind speeds for an AOA of 5.5º is shown in Figures 8(a), (b), and (c). The bulged regime clearly depicts the presence of LSB in the flow field for all the wind speeds considered in the study. A close-view analysis is done in the preceding sections for deeper insight into the flow phenomena. The separation and reattachment region that denotes LSB is shown in Figure 9. Prior to LSB creation, the flow is laminar. However, as it advances towards the trailing edge, it encounters APG, which is why the laminar boundary layer changes its direction, opposite to the flow, after which the velocity vector line increases in length, which is shown clearly in Figure 10. With a reversed velocity vector, the flow separation and reattachment are clearly visible, and the "recirculation zone" denotes the creation of the LSB. The vector length is small at the commencement of flow reversal, increases to its maximum, then decreases further to its minimum, thus re-energizing the flow in the boundary layer. The formation of LSB is found to be happening at 0.46*c* from the leading edge at AOA 5.5º, which is evident in the C_p curve of the simulation results. The flow reattaches to the airfoil's surface and continues as the attached flow as soon as the vector direction returns to its stream-wise direction.

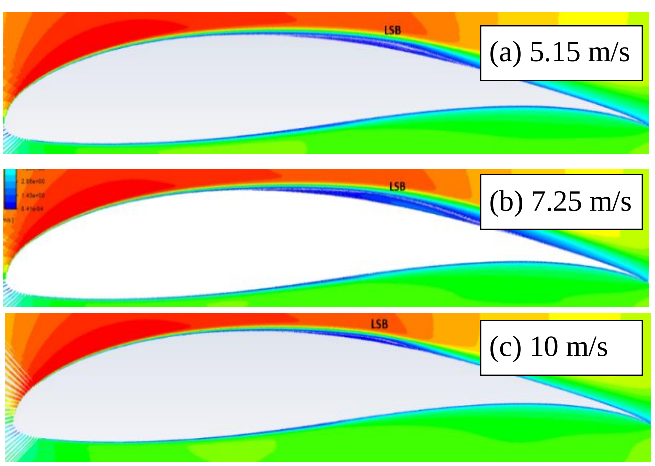

Fig. 8 Velocity vectors above the airfoil are coloured according to their magnitude (red denotes the highest velocity, blue the lowest velocity)

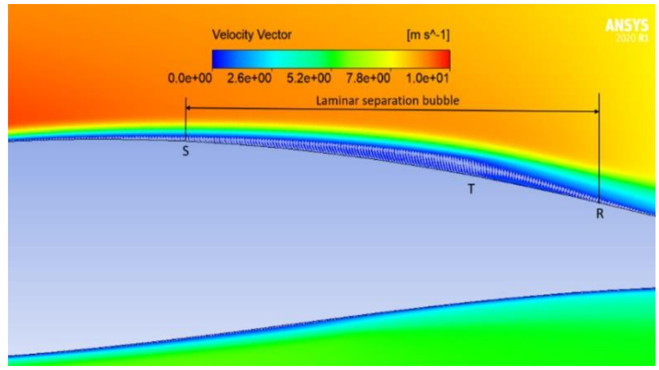

Fig. 9 LSB formation over an airfoil is shown in a velocity vector plot with an AOA of 5.5º. at 5.15 m/s

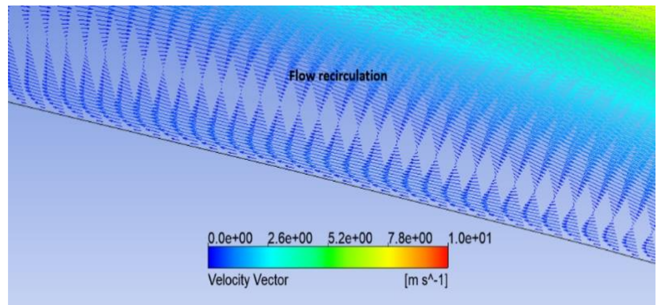

Fig. 10 A close-up of the LSB with the re-circulation region at AOA of 5.5º is shown (The velocity vector line in the left direction is the flow showing the recirculating and transition region)

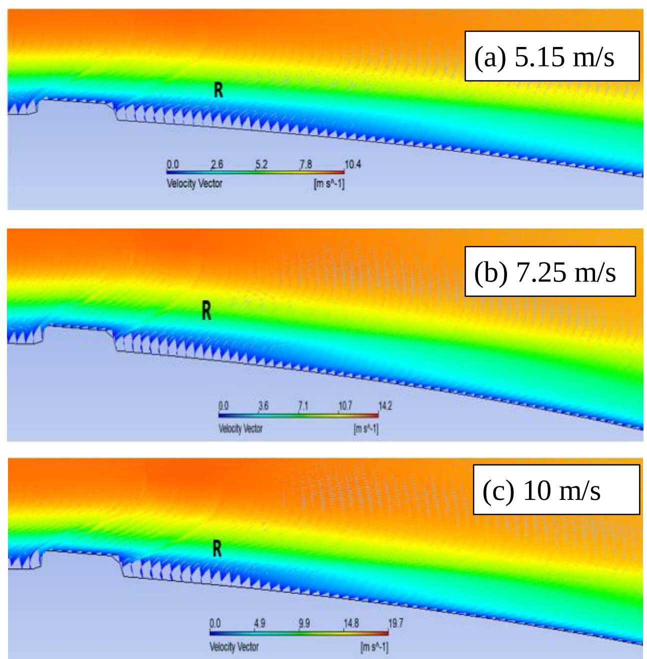

Fig. 11 Velocity vector diagram above the airfoil at AOA 5.5º with different wind speeds (R represents reattachment location) after applying BLT

The velocity vector near the airfoil after applying BLT at different wind speeds is depicted in Figures 11(a) to 11(c). The BLT considerably changes the flow pattern and velocity distribution over the airfoil, as is seen from the vector plot.

The separation and reattachment points are determined by the velocity vector directions. The velocity vectors are in the opposite direction after the BLT, indicating the separated flow. The point of reattachment is reached when the direction of the velocity vectors aligns with the flow direction (represented by R).

This is caused by the boundary layer being re-energized and turbulence being created in the boundary layer over the airfoil. The Turbulent Kinetic Energy (TKE) distributions for the airfoil without BLT at an AOA of 5.5º are shown in Figure 12.

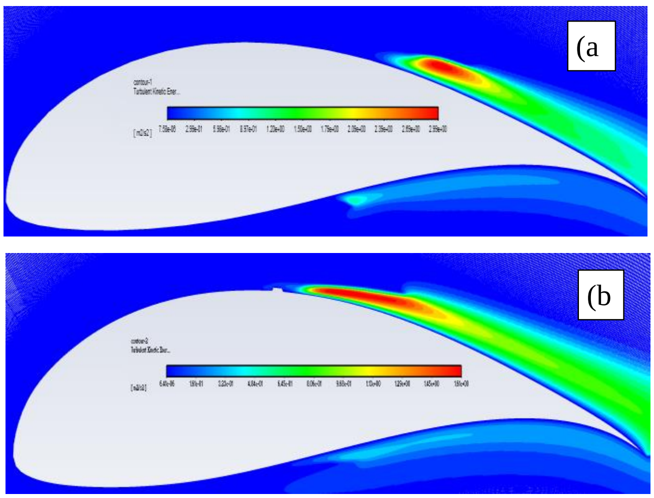

Fig. 12 TKE representation at AOA 5.5º (a) without BLT (b) with rectangular BLT. (5.15 m/s)

An elevated TKE magnitude was visible near the point of reattachment of the flow, which represents the complete transition of laminar flow into turbulent flow following the LSB.

Turbulence is introduced into the flow by the BLT, and the transition into turbulence requires a certain length of flow (transition region). Where the flow reconnects with the airfoil surface following the transition is where the high TKE zone begins.

According to Figure 13(b), the trip energises the flow by mixing effect, transitioning it from laminar to turbulent and eliminating the high turbulent region caused by LSB creation.

No indication of LSB formation is observed for a trip height of 0.3 mm, and the velocity vectors remain attached to the surface of the airfoil after passing over the trip.

3.3. Aerodynamic Performance of FX63-137 Airfoil with Rectangular BLT

The numerical results on the effect of BLT on the drag coefficient (C_d) and drag coefficient to lift coefficient (C_l/C_d), respectively, at different wind speeds (5.15, 7.25 and 10 m s^{-1}) along with its respective baseline results at AOA of 5.5º is shown in Figures 13(a) & (b).

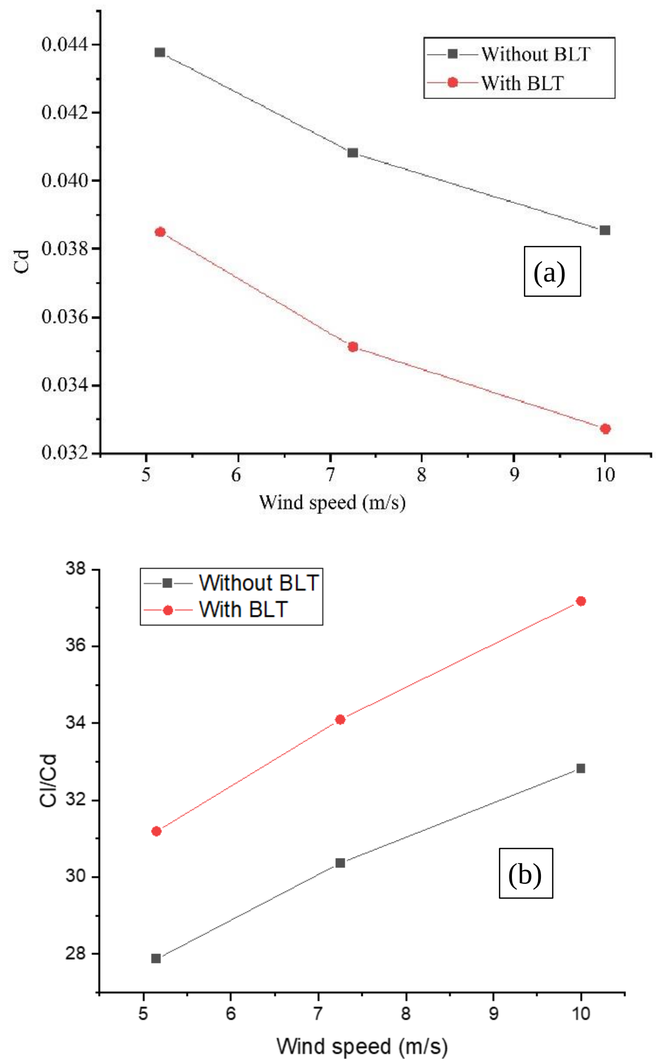

Fig 13 Effect of BLT on (a) C_d, and (b) C_l/C_d at AOA 5.5º at different wind speeds.

A maximum reduction of 14% in C_d and an improvement of 12.3% in C_l/C_d is seen at the design wind speed of 7.25 ms^{-1} at the trip height of 0.3 mm. The boundary layer trip causes the laminar flow to become turbulent when applied to the airfoil. This turbulent flow prevents the formation of LSB as it remains attached to the airfoil surface. Bubble drag is decreased due to the elimination of LSB in this turbulent flow regime. The reduction in bubble drag at BLT outweighs the increase in frictional drag caused by turbulent flow and BLT-induced device drag. Therefore, airfoil with BLT shows better performance when compared to airfoil without it, for 5.15, 7.25 and 10 m/s wind speed. Suppose the BLT height is more than 0.3 mm; the total drag increases (due to increased device drag), depriving the benefit obtained from a reduction in bubble drag [12].

The location of BLT should be optimum as it plays a major role in net reduction in drag. The location of BLT close to LSB will mitigate its formation, whereas being far upstream will result in enhanced frictional drag due to higher turbulent flow length ahead of LSB formation. The selected location of BLT for the current study, i.e. 0.41c from the leading edge where the LSB formed at 0.46c or 0.05c ahead of LSB, is found satisfactory as the net result showed reduced C_d and improved C_l/C_d. The study shows that overall improvement in C_l/C_d can improve power production from the wind turbine blade by applying the BLT technique. The reduction in bubble drag due to the application of the BLT surpasses the increase in frictional drag caused by turbulent flow and BLT-induced device drag. Consequently, the airfoil equipped with BLT demonstrates superior performance compared to the airfoil without it at wind speeds of 5.15, 7.25, and 10 m/s. However, when the BLT height exceeds 0.3 mm, the total drag increases due to greater device drag, negating the benefits gained from reducing bubble drag (Lili Chen et al., 2020).

4. Conclusion

The aerodynamic performance of the FX63-137 airfoil with Boundary Layer Trip (BLT) is evaluated numerically at three different wind speeds (5.15, 7.25 and 10 m/s). The study addresses the formation of Laminar Separation Bubbles (LSB) over the airfoil and the effect of BLT on its performance. The numerical analysis approach is validated using the experimental results available in the literature. The following conclusions are arrived from the present work:

1. The numerical C_p results using the methodology in the present work match well with the literature results.
2. The LSB formation starts at 0.46*c* from the leading edge of the airfoil; the transition from laminar to turbulent flow happens at around 0.6*c*, and the reattachment of flow on the airfoil happens at around 0.73*c* from the leading edge at studied wind speeds.
3. The drag formed due to LSB is eliminated after applying the BLT on the airfoil. After the application of BLT of 0.3 mm height on the airfoil, the total drag decreased by 14%, and a 12.3% net improvement in C_l/C_d was observed at the design wind speed of 7.25 m/s. This shows that C_l has increased and the C_d has decreased, thereby increasing the C_l/C_d ratio.

Acknowledgement

The authors profusely thank Dr. H.M Shivaprasad, Head of the Department, Department of Mechanical Engineering, Dr. Bheemsha Arya, The Principal, BMSCE and Dassault Systems Foundation, for providing necessary facilities.

References

[1] Marcelo M.G. Dias, and Ramiro Gustavo Ramirez Camacho, "Optimization of NREL Phase VI wind Turbine by Introducing Blade Sweep, Using CFD Integrated with Genetic Algorithms," *Journal of Brazilian Society Mechanical Science Engineering*, vol. 44, 2022. [CrossRef] [Google Scholar] [Publisher Link]

[2] H. Dong et al., "Letter: A Note on Flow Characterization of the FX63-137 Airfoil at Low Reynolds Number Using Oil-Film Interferometry Technique," *Physics of Fluids*, vol. 30, no. 10, 2018. [CrossRef] [Google Scholar] [Publisher Link]

[3] Hao Dong et al., "Study on Flow Separation and Transition of the Airfoil in Low Reynolds Number," *Physics of Fluids*, vol. 31, no. 10, 2019. [CrossRef] [Google Scholar] [Publisher Link]

[4] Mustafa Serdar Genç, Kemal Koca, and Halil Hakan Açikel, "Investigation of Pre-Stall Flow Control on Wind Turbine Blade Airfoil Using Roughness Element," *Energy*, vol. 176, pp. 320-334, 2019. [CrossRef] [Google Scholar] [Publisher Link]

[5] Renewables 2020: Analysis and Forecast to 2025, IEA, 2020. [Online]. Available: https://www.iea.org/reports/renewables-2020

[6] IEC 61400-2, Wind Turbines - Part 2: Small Wind Turbines, International Electrotechnical Commission, 2013. [Online]. Available: https://webstore.iec.ch/en/publication/5433

[7] Mohsen Jahanmiri, "*Laminar Separation Bubble: Its Structure, Dynamics and Control*," Chalmers University of Technology, Research Report, pp. 1-24, 2011. [Google Scholar] [Publisher Link]

[8] Meteorologist Jeff Haby, Wind Speed Increasing with Height, The Weather Prediction. [Online]. Available: https://www.theweatherprediction.com/habyhints3/749/

[9] Qing'an Li et al., "Visualization of the Flow Field and Aerodynamic Force on a Horizontal Axis Wind Turbine in Turbulent Inflows," *Energy*, vol. 111, pp. 57-67, 2016. [CrossRef] [Google Scholar] [Publisher Link]

[10] Hailay Kiros Kelele et al., "Characterization of Aerodynamics of Small Wind Turbine Blade for Enhanced Performance and Low Cost of Energy," *Energies*, vol. 15, no. 21, pp. 1-23, 2022. [CrossRef] [Google Scholar] [Publisher Link]

[11] Sher Afghan Khan et al., "Comparing the Effect of Different Turbulence Models on The CFD Predictions of NACA0018 Airfoil Aerodynamics," *CFD Letters*, vol. 12, no. 3, pp. 1-10, 2020. [Google Scholar] [Publisher Link]

[12] Lili Chen et al., "Aerodynamic Performance and Transition Prediction of Low-Speed Fixed-Wing Unmanned Aerial Vehicles in Full Configuration Based on Improved $\gamma - Re\theta$ Model," *Aerospace Science and Technology*, vol. 107, 2020. [CrossRef] [Google Scholar] [Publisher Link]

[13] James F. Manwell, Jon G. McGowan, Anthony L. Rogers, *Wind Energy Explained: Theory, Design and Application*, 2nd ed., John Wiley & Sons, pp. 1-704, 2010. [Google Scholar] [Publisher Link]

[14] John E. Matsson, *An Introduction to ANSYS Fluent 2022*, SDC Publications, pp. 1-688, 2022. [Google Scholar] [Publisher Link]
[15] F.R. Menter, R. Langtry, and S. Völker, "Transition Modelling for General Purpose CFD Codes," *Flow, Turbulence and Combustion*, vol. 77, pp. 277-303, 2006. [CrossRef] [Google Scholar] [Publisher Link]
[16] S.J. Miley, "*Catalog of Low-Reynolds-Number Airfoil Data for Wind-Turbine Applications*," Texas AIM University, Technical Report, pp. 1-626, 2022. [CrossRef] [Google Scholar] [Publisher Link]
[17] Abhijit Mitra, and O.N. Ramesh, "The Role of Laminar Separation Bubbles on the FX 63-137 Airfoil," *Proceedings of the International Conference on Instability and Control of Massively Separated Flows*, Prato, Italy, pp. 51-56, 2015. [CrossRef] [Google Scholar] [Publisher Link]
[18] W.D. Musial, and D.E. Cromack, "Influence of Reynolds Number on Performance Modeling of Horizontal Axis Wind Rotors," *Journal of Solar Energy Engineering*, vol. 110, no. 2, pp. 139-144, 1988. [CrossRef] [Google Scholar] [Publisher Link]
[19] Christian V. Rodriguez, and Cesar Celis, "Design Optimization Methodology of Small Horizontal Axis Wind Turbine Blades Using a Hybrid CFD/BEM/GA Approach," *Journal of the Brazilian Society of Mechanical Sciences and Engineering*, vol. 44, 2022. [CrossRef] [Google Scholar] [Publisher Link]
[20] Ronit K. Singh et al., "Design of a Low Reynolds Number Airfoil for Small Horizontal Axis Wind Turbines," *Renewable Energy*, vol. 42, pp. 66-76, 2012. [CrossRef] [Google Scholar] [Publisher Link]
[21] Michael S. Selig, and Bryan D. McGranahan, "Wind Tunnel Aerodynamic Tests of Six Airfoils for Use on Small Wind Turbines," *Journal of Solar Energy Engineering*, vol. 126, no. 4, pp. 986-1001, 2004. [CrossRef] [Google Scholar] [Publisher Link]